Self-assembled pullulan–silica oxygen barrier hybrid coatings for food packaging applications

Journal:	*Journal of Agricultural and Food Chemistry*
Manuscript ID:	jf-2011-04033d.R1
Manuscript Type:	Article
Date Submitted by the Author:	n/a

Complete List of Authors:	Farris, Stefano; University of Milan, Food Science and Microbiology Introzzi, Laura; University of Milan, Food Science and Microbiology Fuentes-Alventosa, José María; Centro de Investigación y Formación Agraria "Alameda del Obispo", Instituto de Investigación y Formación Agraria y Pesquera (IFAPA) Santo, Nadia; University of Milan, Interdepartmental Center of Advanced Microscopy Rocca, Roberto; Metalvuoto Spa, Piergiovanni, Luciano; University of Milan, Food Science and Microbiology

Self-assembled pullulan–silica oxygen barrier hybrid coatings for food packaging applications

Stefano Farris[*a], Laura Introzzi[a], José Maria Fuentes-Alventosa[a,b], Nadia Santo[c], Roberto Rocca[d], Luciano Piergiovanni[a]

[a] *DiSTAM, Department of Food Science and Microbiology, Packaging Division, University of Milan, Via Celoria 2 – 20133 Milan, Italy*

[b] *Centro de Investigación y Formación Agraria "Alameda del Obispo". Instituto de Investigación y Formación Agraria y Pesquera (IFAPA). Avda. Menéndez Pidal s/n. 14004 Córdoba, Spain*

[c] *Interdepartmental Center of Advanced Microscopy, CIMA, University of Milan Via Celoria 26 – 20133 Milan, Italy*

[d] *Metalvuoto Spa, Via L. da Vinci 3 – 20040 Milan, Italy*

*Corresponding author. Tel.: +39 0250316654; Fax: +39 0250316672

Email address: stefano.farris@unimi.it (S. Farris)

ABSTRACT. The scope of this study encompassed the evaluation of pullulan as a suitable biopolymer for the development of oxygen barrier coatings to be applied on polyethylene terephthalate (PET), especially for food packaging applications. To enhance the oxygen barrier properties of the organic phase (pullulan) even at high relative humidity values, an inorganic phase (silica), obtained through *in situ* polymerization, was also utilized to obtain hybrid coatings using the sol-gel technique. Transmission electron microscopy (TEM) images and Fourier transform infrared (FT-IR) spectra showed that mixing the two phases yielded a three-dimensional hybrid network formed by self-assembly and mediated by the occurrence of new hydrogen bond interactions at the inter-molecular level, although the formation of new covalent bonds could not be excluded. The deposition of the hybrid coatings decreased the oxygen transmission rate (OTR) of the plastic substrate by up to two orders of magnitude under dry conditions. The best performance throughout the scanned humidity range (0%–80% relative humidity) was obtained for the formulation with the lowest amount of silica (that is, an organic/inorganic ratio equal to 3).

KEYWORDS: Fourier transform infrared (FT-IR) spectroscopy; oxygen transmission rate (OTR); packaging; pullulan; transmission electron microscopy (TEM)

Introduction

Pullulan, an exopolysaccharide (EPS) produced by the yeast-like forms of the fungus *Aureobasidium pullulans*, is a regularly repeating copolymer {→6)-α-D-glucopyranosyl-(1→4)-α-D-glucopyranosyl-(1→4)-α-D-glucopyranosyl-(1→}$_n$, that can be viewed as a succession of α-(1→6)-linked (1→4)-α-D-triglucosides, that is, maltotriose (G_3) (*1*) (Figure 1). The alternation of (1→4) and (1→6) bonds is responsible for the two principal features of pullulan, namely structural flexibility (centered on the α-1→6-linkages) and enhanced solubility (*2,3*). The hydroxyl groups extensively distributed along its skeleton not only enable pullulan to easily establish hydrogen bonds with other polar molecules, but also make this polysaccharide suitable for many derivatizations, including esterification, etherification, hydrogenation, and carboxylation (*4*).

Pullulan is soluble in both cold and hot water, insoluble in organic solvents, odorless, tasteless, non-toxic, and biodegradable, with good adhesive and binding properties as well as oxygen barrier properties under dry conditions (*5*). The main applications of pullulan pertain to the health care (lotions, shampoos, oral care), pharmaceutical (denture adhesives, capsules for dietary supplements, sustained-release formulations), and food (binder and stabilizer in food pastes, edible films, and protective glaze on foods) industries (*6*). More advanced applications include the recent development of pullulan-based antimicrobial active packaging systems (*7*) and pullulan-functionalized electrospun nanofibers (*8*).

In spite of its appealing peculiarities and all of the aforementioned applications, pullulan is still an under-exploited biopolymer, mainly due to its high cost. Currently, pullulan is quoted at 28 €/kg, that is, approximately three times higher than the price of other polysaccharides, such as dextran and xanthan, and approximately five times higher than the price of a synthetic oil-

derived oxygen barrier polymers, such as polyvinyl alcohol (PVOH). The removal of melanin pigments during the downstream process and the limited scale of pullulan production are the two major factors that determine production costs (*6*). Therefore, new enhanced strains, engineering innovations, and novel applications might improve the economics of pullulan production and expand its market penetration.

Among other opportunities, the food packaging field is being considered with renewed interest, in particular with respect to the development of bio-based materials (*9*). In this respect, coating technology has attracted (and still attracts) the attention of many researchers attempting to obtain structures with either new features (e.g., antimicrobial coatings) (*10*) or improved properties (e.g., barrier properties) (*11*). Coating technology applied to biomacromolecules involves the use of water solutions/dispersions with a concentration ranging approximately from 3 wt.% to 15 wt.% depending on the characteristics (e.g., molecular weight) of the selected molecule. These solutions are then deposited onto different substrates (e.g., flexible plastic films) through different techniques, among which the gravure coating technique seems to afford a number of advantages over other techniques (e.g., reverse roll coaters, calendar coaters, knife-over-roll coaters, blade coating, wire-wound rod coater). One important advantage is that he removal of the solvent, generally achieved by hot air and infrared lamps, is facilitated by the thin coating thickness achieved by gravure coating (usually from 0.2 to 2 μm) (*12*).

The development of new oxygen barrier biopolymer coatings for plastic substrates is becoming an intriguing field of application, especially in view of the possibility of replacing commonly used synthetic polymers (for example, PVOH, ethylene vinyl alcohol – EVOH, and polyvinylidene chloride – PVDC) with new formulations originating from agricultural and renewable resources (*13*). This approach has also been suggested as a valuable and promising

way to manage waste disposal issues (*14*). Owing to its inherent good oxygen barrier properties, pullulan is a valid candidate for the design of new coatings, and would be specifically suitable for the protection of readily oxidized fats and vitamins in foods. However, before this goal can be achieved, a major drawback needs to be addressed: its water sensitivity, due to the hydrophilic hydroxyl groups distributed along the pullulan backbone (*15*). Therefore, to make these biopolymer coatings successful for a broader range of relative humidity (which appears to be more realistic than a fixed-humidity condition), further research in this area must be encouraged.

The aim of this study was to develop coatings for conventional plastic packaging materials using pullulan as the organic phase to provide the necessary oxygen barrier, in combination with tetraethoxysilane (TEOS), a metal alkoxide precursor of silica used as the inorganic counterpart and intended to provide resistance to humidity. The hypothesis was that pullulan can successfully mimic organic, petrol-derived polymers in its interaction with the inorganic phase to form high oxygen barrier hybrid coatings. Based on the literature, this is the first work envisaging the use of pullulan as a biopolymer coating directly applied on a plastic substrate. This could pave the way for a new alternative to the petrol-based coatings currently available on the market of food packaging plastics.

Fundamental chemistry underlying *in situ* development of pullulan–silica hybrids

Some aspects of theory linked to metal alkoxide chemistry and its potential interactions with pullulan are summarized hereinafter to better clarify the justifications of this study. The significant chemical reactions involved in the formation of the hybrid network between TEOS and pullulan are summarized in Figure 2. The hydrolysis of the metal alkoxide, which is the first step of the overall reaction, occurs due to the nucleophilic attack of the oxygen contained in water on silicon atoms (*16*). However, protonation of the alkoxide groups is faster if an acid

(e.g., HCl) is used as a catalyst (*17*), although base-catalyzed hydrolysis is also well established (*18*). Owing to the hydrolysis reaction, the alkoxide groups (-OR) are replaced with hydroxyl groups (-OH) to form silanol compounds, $Si(OH)_n$, where ethanol is the by-product. Upon hydrolysis, the $Si(OH)_n$ groups may react according to a typical condensation scheme by two different routes (water condensation and alcohol condensation) to yield in both cases SiO_2 covalent bonds and either water or alcohol as by-products. However, due to molecular constraints, Si–O–Si linkage formation is typically about 80–85% of the theoretical value (*19*). In the presence of pullulan, in addition to the condensation reactions, $Si(OH)_n$ groups arising from TEOS can interact via hydrogen bonds with the pendant polar groups (e.g., hydroxyl groups) along the backbone of the biopolymer to yield the hybrid network as reported in the downwards scheme of Figure 2. The formation of covalent bonds between the hydroxyl groups and the silanol groups has also been postulated (*20,21*). Whether these two routes (i.e., the condensation reaction and hydrogen bond formation) proceed simultaneously or not depends strictly on many factors, and relies especially on the concentration of the reagents and the pH of the medium. The expected final result is a new material that should share the attributes of each individual phase, such as the oxygen barrier property of pullulan and the resistance to moisture of the glass-like inorganic component.

Experimental Section

Materials. High purity tetraethoxylane (Sigma-Aldrich, Milan, Italy) was used as the metal alkoxide precursor of the inorganic phase; 1 M hydrochloric acid (Sigma-Aldrich, Milan, Italy) was used as the catalyst; pullulan powder (PF-20 grade, M_n ~ 200 kDa; Hayashibara Biochemical Laboratories Inc., Okayama, Japan) was employed as the organic system. All materials were used as received for the preparation of the hybrid solution. Ethanol (96% $^{v}/_{v}$;

Sigma-Aldrich, Milan, Italy) and Milli-Q water (18.3 MΩ · cm) were used as the only solvents throughout the experiments. Reagent grade lithium chloride anhydrous (LiCl), potassium acetate (CH_3COOK), magnesium chloride hexahydrate ($MgCl_2 \cdot 6H_2O$), potassium carbonate (K_2CO_3), magnesium nitrate hexahydrate [$Mg(NO_3)_2 \cdot 6H_2O$], lithium acetate dihydrate ($C_2H_3LiO_2 \cdot 2H_2O$), sodium chloride (NaCl), potassium nitrate (KNO_3) (Sigma-Aldrich, Milan, Italy) were all used to prepare the saturated salt solutions, giving theoretical water activity (a_w) values of 0.11, 0.23, 0.32, 0.44, 0.52, 0.66, 0.75, and 0.92 at 25 ± 0.2°C , respectively.

Preparation of hybrid coatings. In the first step, an acidic (pH = 2.0 ± 0.8) hydroalcoholic (30 wt-% ethanol) solution of TEOS was prepared by using 1 M HCl (0.78 wt-%) as a catalyst. In this step, the H_2O:TEOS molar ratio was fixed at 4:1. The hydrolysis of TEOS was carried out at room temperature for approximately 1 hour. At the same time, a water dispersion of pullulan was prepared at room temperature according to the concentrations reported in Table 1 by mixing the polysaccharide with the solvent by means of rapid stirring (1500 rpm x 1 hour). The pH of the final pullulan water dispersions ranged between 5.0 ± 0.05 for the highest pullulan concentration (i.e., formulation H_0) and 5.65 ± 0.08 for the lowest pullulan concentration (i.e., formulation $H_{0.5}$). In the second step, the inorganic and organic phases were mixed together for 1 hour, in order to allow the formation of the hybrid network. The composite solutions were then deposited by roll-coating onto 12 ± 0.5 μm-thick polyethylene terephthalate (PET) films (Toray Saehan, Kyungbuk, South Korea) using an automatic applicator (Ref. 1137; Sheen Instruments, Kingston, UK), equipped with a steel horizontal wire-wound rod of 18 cm width (Ref. 1120; Sheen Instruments, Kingston, UK), to obtain a wet coating thickness of approximately 10 μm (data provided by the factory). Coating deposition was performed according to ASTM D823-07 – Practice C (*22*), at a constant speed of 150 mm min^{-1}. With the goal of investigating the

influence of the organic/inorganic ratio [O/I, defined as the pullulan/$(SiOH)_4$ weight ratio for a complete hydrolysis process] on the final oxygen barrier properties of the hybrid coatings, six different solutions were prepared by varying the O/I ratio of the coating from 100/0 to 50/100, as reported in Table 1. Both solvent evaporation and the progress of the reactions leading to the hybrid network formation were obtained by storing the coated PET films in a vacuum oven at 40°C for 24 hours.

Residual moisture. The residual moisture of the coatings after drying was measured by means of a halogen moisture analyzer, mod. HG63 (Mettler Toledo, Zurich, Switzerland).

Thickness determination. A 10 × 10 cm sample (plastic substrate + coating) was cut and weighed (M_1, g). The coating was then mechanically removed by immersion in hot water (80°C) and the resulting substrate film was weighed (M_2, g). The apparent thickness (μm) of the coating was obtained according to the following equation (*14*):

$$l = \frac{M_1 - M_2}{\rho} \times 100 \quad (1)$$

where ρ (g cm^{-3}) is the density of the aqueous dispersion. Three replicates were analyzed for each biopolymer composition. In order to check for the consistency of the obtained results, the thickness of both uncoated and coated PET films was also measured with a micrometer (Dialmatic DDI030M; Bowers Metrology, Bradford, UK) to the nearest 0.001 mm at 10 different random locations. Finally, a rough indication of the thickness of both coatings and substrate was achieved using an optical microscope (OM) (Micro Nikon Eclipse ME600 Laboratory Imaging; Nikon Instruments, Sesto Fiorentino, Italy) at 50× magnification (Figure 3). In this case, films after storage in the vacuum oven were fixed on a rectangular steel sample holder and a sharp razor blade was then used to cut them lengthwise, permitting the observation of the cross section

of the composite films. Finally, the thickness of the layers was measured using NIS-Element software (Nikon Instruments, Sesto Fiorentino, Italy).

Fourier Transform Infrared – Attenuated Total Reflectance (FTIR-ATR). The structural characteristics and chemical bonding of the coatings at different O/I ratios were investigated by a PerkinElmer FT-IR Spectrum 100 Series spectrometer (PerkinElmer, Waltham, MA, USA) equipped with a universal attenuated total reflectance (UATR) accessory featuring a single-reflection sampling plate with a 1.8 mm round germanium surface. To ensure satisfactory physical contact took place between the samples and the crystal surface, a high-pressure clamping device was used. Spectra were recorded at room temperature within the range of 650–4000 cm^{-1} at 4 cm^{-1} resolution. Spectrum 6.0 software was used for data acquisition and analysis.

Moisture sorption properties. To provide evidence of improved moisture resistance of the hybrid coatings compared to the pure pullulan coatings, moisture sorption data were collected according to the procedures reported in the COST project of European Cooperation in the field of Technical and Scientific Research and the principles described by Bell and Labuza (*23*). For this purpose, approximately 4 g of each coating formulation were initially kept for three weeks in a glass desiccator containing Drierite®, and then moved to sealed glass jars containing saturated salt slurries in the a_w range of 0.11 to 0.92 and stored in a refrigerated incubator (mod FOC 225E; Velp Scientifica, Usmate, Italy) at 25 ± 0.2°C. For all samples, equilibrium was reached in two weeks. The equilibrium moisture content data were then fitted to the Guggenheim–Anderson–DeBoer (GAB) sorption isotherm model:

$$M = \frac{CKM_0}{[(1-Ka_w)(1-Ka_w+CKa_w)]}a_w \quad (2)$$

using nonlinear curve-fitting software (Tablecurve 4.0; Jandel Scientific, San Rafael, CA). In Equation (2), M and M_0 are the equilibrium moisture content and the moisture content value in

the monolayer, respectively, both expressed as g/100 g of dry matter. *C* and *K* are constants associated with the enthalpies of sorption of the monolayer and multilayer, respectively. In particular, the constant *C* should always have a positive value, due to the exothermic interaction of water vapor with the primary sorption sites of the hygroscopic matrix, whereas reasonable values of *K* considerably higher than unity have been never found in the literature. Therefore, the validity of the mathematical model assumed in this work was assessed not only by evaluating its ability to fit the experimental data (hence by the R^2 coefficient), but also assuming the physicochemical basis of the water sorption phenomenon.

Microscopy analyses. Transmission electron microscopy (TEM) images were captured to visualize the individual phases (i.e., the inorganic SiO_2 and the organic pullulan phases) as well as hybrid network growth. For this purpose, 5 μL of the hybrid dispersions were deposited onto a Formvar-coated Cu grid (400-mesh). After adsorption, the grid was stained with a droplet (5 μL) of 1% uranyl acetate and dried with filter paper. Observations were made using a LEO 912 AB energy-filtering transmission electron microscope (EFTEM) (Carl Zeiss, Oberkochen, Germany) operating at 80 kV. Digital images were recorded with a ProScan 1K Slow-Scan CCD camera (Proscan, Scheuring, Germany).

The global organization of coated surfaces and the possible presence of fractures on the coated layers were visualized using an optical microscope (OM) (Micro Nikon Eclipse ME600 Laboratory Imaging; Nikon Instruments, Sesto Fiorentino, Italy) at 10× magnification. Pieces of coated films (30 × 10 mm) after storage in the desiccator were fixed on a rectangular steel sample holder and observed without any pre-treatment. Image capture and refining were carried out using NIS-Element software (Nikon Instruments, Sesto Fiorentino, Italy).

Oxygen barrier properties. The oxygen barrier properties of both uncoated and coated PET films were assessed on a 50 cm^2 surface sample using a MultiPerm permeability analyzer (ExtraSolution® Srl, Navacchio, Italy), according to the standard method ASTM F2622-08 (*24*), with a carrier flow (N_2) of 10 mL min^{-1}. With the goal of quantifying the influence of the external relative humidity conditions on the barrier properties of coated films, measurements were performed at 23°C and at five different relative humidity conditions (i.e., 0%, 20%, 40%, 60%, and 80% RH). The results were expressed as the oxygen transmission rate (OTR, mL m^{-2} 24 h^{-1} at one atmosphere pressure difference), which has been indicated as the most suitable unit for heterogeneous packaging materials (e.g., multilayer and coated films), that is, whenever a linear relationship between permeability and thickness is not maintained (*25*). The final OTR values were from three replicates.

Statistical analysis

The statistical significance of differences in the properties and behaviors of coated films was determined by one-way ANOVA, using JMP 5.0.1 software (SAS Campus Drive, Cary, NC). The mean values, where appropriate, were compared by Student's *t*-test with a significance level (p) < 0.05.

Results and Discussion

Residual moisture and coating thickness. As can be seen from the data reported in Table 1, solvent removal upon drying was almost complete regardless of the specific coating formulation.

Therefore, the differences detected in the thickness values of the hybrid coatings (Table 1), despite the same solid content equal to 10 wt-%, can be explained considering the increased amount of ethanol (the by-product of the hydrolysis and condensation reactions) as the O/I ratio

decreased. The dilution effect arising from ethanol was thus reflected in the reduced thickness of the hybrid coatings with a higher inorganic phase content.

FTIR–ATR analysis. The FTIR–ATR analyses are summarized in Figure 4. Figure 4a and Figure 4b display the spectra of coatings collected from pure pullulan and from reacted TEOS (i.e., after hydrolysis and condensation), with the characteristic peaks associated with specific bands in evidence (*26,27*). Figure 4c and Figure 4d display the two most significant spectral regions where changes occurred in the hybrid coatings at different O/I ratios. An overall visualization of all spectra in the investigated range of 650–4000 cm^{-1} is provided in the supporting information (see Figure S1). In Figure 4b, the presence of peaks associated with silanol groups (~ 945 cm^{-1}) and silica (~ 1060 cm^{-1} and ~ 800 cm^{-1}) was clear evidence of the occurrence of both hydrolysis and condensation reactions on the metal alkoxide. The spectra collected from hybrid coatings showed some important changes compared to the pure phases. In the 980 cm^{-1} – 880 cm^{-1} region (Figure 4c), a band including the two overlapping peaks—corresponding to the silanol groups of TEOS and the α-(1→6) linkages of pullulan—gradually shifted toward higher wavenumbers as the inorganic phase increased. In addition, as the inorganic phase concentration increased, the peak centered at around 945 cm^{-1} became increasingly sharper compared to that of reacted TEOS. Correspondingly, the band of the hybrid coatings at around 3300 cm^{-1} (Figure 4d and Figure S1), associated with hydroxyl group stretching, became broader compared to that of pullulan, while the peak slightly shifted toward lower wavenumbers. It has been pointed out that the simultaneous broadening and shifting of peak absorption area is possibly due to extensive hydrogen bonding between the silanol and hydroxyl groups of the organic phase (*28–30*). Another indication of the interaction between the hydroxyl groups of pullulan and silanol groups through hydrogen bonds was observed with the

peak centered at 1081 cm^{-1} for pure pullulan (Figure 4c). As the inorganic concentration increased, a slight shift toward lower wavenumbers (up to 1076 cm^{-1} for the $H_{0.5}$ hybrid coatings) occurred, suggesting the possible participation of the hydroxyl groups on C_6 of the pullulan backbone in hydrogen bond formation.

Interestingly, the strong sharp band of pullulan at 1021 cm^{-1} was visible up to the hybrid H_1, whereas it appeared as a weak shoulder in hybrid coatings $H_{0.75}$ and $H_{0.5}$. These latter two, conversely, showed a more pronounced peak at around 1047 cm^{-1} (i.e., halfway between the two main peaks of reacted TEOS and pullulan, respectively), which apparently seems to be related to the unknown shoulder barely visible in the pullulan spectrum a few wavenumbers before the main peak at 1021 cm^{-1}. A tentative explanation for the appearance of this new peak could be related to the formation of new covalent bonds between the silanol groups and the hydroxyl groups of pullulan. The new peak would thus be associated with the Si–O stretching vibration of the newly formed Si–O–C linkage. Although the formation of new covalent bonds between the silanol groups arising from the hydrolysis of TEOS and the pendant hydroxyl groups of an organic phase (e.g.,. polyvinyl alcohol) has been claimed (*21,28*), that hypothesis is premature at this time and needs further experimental confirmation.

Moisture sorption isotherms

Moisture sorption isotherms for samples H_0 (pure pullulan coating), H_3, and H_2 are reported in Figure 5. For the three curves, the moisture uptake increased monotonically until a specific a_w (~ 0.7) was reached. Above this point, moisture gain rose dramatically due to the dissolution of the crystalline domains by water molecules, which interacted via hydrogen bonds with the hydroxyl groups involved in the formation of the crystalline phase (*24*). Given that this kind of sorption is mainly driven by surface effects, the dimension of the sample exposed to moisture is a key factor

for proper interpretation of the water content as a function of a_w. This is why, owing to the extensive shrinking seen in the specimens, which produced specimens of small size after evaporation of the solvent, the moisture sorption properties of the hybrid coatings H_1, $H_{0.75}$, $H_{0.5}$ were not assessed.

Figure 5 also shows that a lower moisture content for any given a_w value was observed for the hybrid coatings H_3 and H_2, indicating the 'protective' effect of the inorganic phase toward the surrounding moisture. This was also confirmed by the modeling data (Table 2) arising from the fitting procedure of Equation 2 to the experimental sorption measurements. In particular, the moisture content in the monolayer (M_0) predicted by the GAB model was equal to 0.78, 0.53, and 0.19 g/100 g solids for samples H_0, H_3, and H_2, respectively, which was consistent with the different silica content of the samples.

Hybrid network formation and morphology. Representative TEM images of pure silica, pullulan and the hybrid coating H_1 are presented in Figures 6a–d, respectively. Figure 6a displays the SiO_2 network after hydrolysis and condensation of the metal alkoxide precursor (i.e., TEOS). As can be seen readily, the inorganic network was formed by silica particles approximately 30–50 nm in diameter and well interconnected with one another to form a very tight, compact and ordered structure, which is reflected in the typical high rigidity of silica coatings. Conversely, pullulan molecules (Figure 6b) appeared as thin chains with an estimated diameter of approximately 5–7 nm, with more disordered organization and a remarkable extent of intermolecular folding (entanglement), indicators that have to be linked to the flexibility of high molecular weight chains. The association of the two phases (i.e., organic and inorganic) led to a new scenario. As the O/I ratio increased, the silica network partially lost its original configuration (Figure 6c), being gradually 'disassembled' by the 'permeating' organic phase.

This seems to be confirmed by the image displayed in Figure 6d, where the larger-size silica clusters appear to be twisted by pullulan chains. However, the latter are hardly visible in the same figure (they look like bright ridges), due to the much higher sensitivity of silica to electrons compared to organic molecules. This disaggregation/disruption of the silica network finally led to a more segregated, web-like pattern. Presumably, the reason for this lies in the fact that the addition of pullulan promoted an increase in the pH of the original TEOS hydroalcoholic solution. It is well established that pH is a pivotal factor in determining the evolution of silica networks, and thus their final morphology. In particular, it has been pointed out that an increase in pH yields less-compact networks, with increased inter-chains space (*31*). The final silica–pullulan structure can thus be conceived as a self-assembled three-dimensional hybrid network, where the organic and inorganic phases interact spontaneously through intermolecular hydrogen bonding, as also shown by FTIR-ATR.

Oxygen barrier properties. The experimental results on the barrier properties are summarized in Table 3, whereas the OTR evolution throughout the ΔRH (%) range of the uncoated substrate (PET), pristine pullulan (H_0) and the five hybrid coatings considered in this work is displayed in Figure 7. At first glance, it can be seen that all hybrid coatings provided a reduction in the oxygen transmission rate compared to the neat substrate (PET), at least up to 60% relative humidity (the permeability decrease of PET at high relative humidity is well known and has been described elsewhere) (*32,33*). In particular, formulation H_3 provided, under dry conditions, a remarkable OTR value below 1 mL m^{-2} 24 h^{-1}, which is a typical value of high barrier coatings used within the food packaging field. In addition, the H_0, H_3, H_2, and H_1 coatings exhibited a similar trend, while the $H_{0.5}$ hybrid coating behaved more similarly to the plastic substrate, at least in the 0%–40% RH range. The behavior of the $H_{0.75}$ coating was similar to that of the

plastic substrate at up to 40% RH, while it followed the same trend of the other coatings above that point. These results clearly demonstrate that increasing the inorganic concentration had a detrimental effect on the barrier properties of the final structure. This is in contrast to what was expected, as it is well established that decreasing the O/I ratio should improve the barrier properties, assuming oxygen permeation occurs mainly or exclusively within the organic phase (*34*). Causes linked to the physical changes induced by the increase in the O/I ratio on the overall organization of the final coatings should be invoked to explain the obtained results.

The optical microscope images of the surface of the hybrid coatings (Figure 8) allowed for some important observations, otherwise unattainable by simple visual inspection of the samples (also due to the very high transparency of the films). Besides the pure pullulan coating, whose high surface smoothness has already been reported elsewhere (*35*), the only sample with an even, smooth surface, with no evidence of either cracks or pinholes, was the H_3 hybrid. The surface of the H_2 sample exhibited some bright veins, which appeared to be organized in a denser and more regular pattern in the H_1 sample, as clearly highlighted by the topographical image. Whether these veins are due to molecular re-organization or whether they represent the first sign of surface failure is still not clear. In the $H_{0.75}$ and $H_{0.5}$ samples, the inherent rigidity of the silica network prevailed on the innate flexibility of pullulan, insomuch as ruptures occurred on the coating surface, particularly evident in sample $H_{0.5}$. These ruptures appeared as parallel cracks of ~ 10 μm width and separated by ~ 100 μm one from the other, suggesting that they probably formed along the tracks of the wires of the rod used to lay the coating dispersion on the plastic substrate. The main reason presumably lies in the mechanical stresses triggered by the shrinking of the matrix during the solvent evaporation step, as also reported by many authors (*29,36,37*).

Ruptures and cracks dramatically affected the oxygen barrier properties of the final structure for two main reasons. On the one hand, they acted as gaps where the permeation of oxygen was no longer governed by the physicochemical properties of the coating, but by the performance of the plastic substrate. This is why the oxygen transmission rate of the coatings increased with decreasing O/I ratios, approaching the value of the underlying PET substrate. On the other hand, it is well known that cracks and pinholes play an important role as amplifiers for water vapor penetration inside the coating network, thus accelerating the swelling phenomenon, which in turn will affect the final oxygen barrier properties. This is probably the main reason why all of the hybrid coatings tested in this work completely lost their barrier performance at 80% relative humidity. Therefore, in light of the obtained results, it can be said that although all of the formulations tested led to some extent to a reduction in OTR values (ranging from ~ 99% to ~ 27%) compared to the PET substrate, the hybrid coating with the lowest silica content achieved the best performance, fully comparable to those reported in the literature for similar organic/silica hybrid coatings, at least up to 60% relative humidity (*24,34*).

In conclusion, this study has demonstrated that pullulan, in combination with TEOS, can be profitably used to generate oxygen barrier hybrid coatings. As demonstrated by TEM and spectrometric analyses, the formation of a hybrid network through self-assembly is driven by inter-molecular hydrogen bond formation at the interfaces of end-capped silanol groups generated from TEOS and of the pendant hydroxyl groups of the pullulan backbone. However, it is necessary to use the lowest amount of silica to avoid extensive cracking of the coatings, thus preserving the ‘protective’ effect of the inorganic phase toward the surrounding humidity. Eventually, this would allow the achievement of OTR values fully comparable to the current solutions available on the market, making pullulan, in association with silica, a viable alternative

to the commonly used organic polymers derived from petrol for the development of oxygen barrier coatings, especially as intended for food packaging applications.

Although this new application may be beneficial with regard to expanding the market penetration of pullulan, its cost still represents a remarkable obstacle. Based on the latest quotation of each component, the unit cost of PET film (12 μm) coated with the H_3 formulation is estimated at 3.7 €/kg, which is higher than the sale price of the today's oil-derived alternatives (e.g., the price of PET 12 μm coated with PVOH 1.0 μm is ~ 2.6 €/kg).

Literature cited

(1) Leathers, T. D. Pullulan. In *Polysaccharides II: Polysaccharides from Eukaryotes*; Vandamme, E. J.; De Baets, S.; Steinblichel, A., Eds.; Wiley-VCH: Weinheim, Germany, 2002; Vol. 6, pp. 1–35.

(2) Buliga, G. S.; Brant, D. A. Temperature and molecular weight dependence of the unperturbed dimensions of aqueous pullulan. *Int. J. Biol. Macromol.* **1987,** *9,* 71–76.

(3) Dais, P.; Vlachou, S.; Taravel, F. ^{13}C nuclear magnetic relaxation study of segmental dynamics of the heteropolysaccharide pullulan in dilute solutions. *Biomacromolecules* **2001,** *2,* 1137–1147.

(4) Shingel, K. I. Current knowledge on biosynthesis, biological activity, and chemical modification of the exopolysaccharide, pullulan. *Carbohyd. Res.* **2004,** *339,* 447–460.

(5) Yuen, S. Pullulan and its applications. *Process Biochem.* **1974,** *9,* 7–9.

(6) Leathers, T. D. Biotechnological production and applications of pullulan. *Appl. Microbiol. Biotechnol.* **2003,** *62,* 468–473.

(7) Trinetta, V.; Cutter, C. N.; Floros, J. D. Effects of ingredient composition on optical a mechanical properties of pullulan film for food-packaging applications. *Food Sci. Technol.-Leb.* **2011,** *44,* 2296–3301.

(8) Islam, M. S.; Akter, N.; Karim, M. R. Preparation of superhydrophobic membranes by electrospinning of fluorinated silane functionalized pullulan. *Colloid. Surface. A* **2010,** *362,* 117–120.

(9) Sanchez-Garcia, M.D.; Hilliou, L.; Lagaron, J. M. Nanobiocomposites of carrageenan, zein, and mica of interest in food packaging and coating applications. *J. Agric. Food Chem.* **2010,** *58,* 6884–6894.

(10) Ben Arfa, A.; Preziosi-Belloy, L.; Chalier, P.; Gontard, N. Antimicrobial paper based on a soy protein isolate or modified starch coating including carvacrol and cinnamaldehyde. *J. Agric. Food Chem.* **2007,** *55,* 2155–2162.

(11) Han, J.; Salmieri, S.; Le Tien, C.; Lacroix, M. Improvement of water barrier property of paperboard by coating application with biodegradable polymers. *J. Agric. Food Chem.* **2010,** *58,* 3125–3131.

(12) Farris, S.; Schaich, K. M.; Liu, L. S.; Piergiovanni, L.; Yam, K. L. Development of polyion-complex hydrogels as an alternative approach for the production of bio-based polymers for food packaging applications: a review. *Trends Food Sci. Tech.* **2009,** *20,* 316–332.

(13) Liu, L. S.; Finkenstadt, V. L.; Liu, C.-K.; Jin, T.; Fishman, M. L.; Hicks, K. B. Preparation of poly(lactic acid) and pectin composite films intended for applications in antimicrobial packaging. *J. Appl. Polym. Sci.* **2007,** *106,* 801–810.

(14) Farris, S.; Introzzi, L.; Piergiovanni, L. Evaluation of a bio-coating as a solution to improve barrier, friction and optical properties of plastic films. *Packag. Technol. Sci.* **2009,** *22,* 69–83.

(15) Guilbert, S.; Gontard, N. Agro-polymers for edible and biodegradable films: review of agricultural polymeric materials, physical and mechanical characteristics. In *Innovations in Food Packaging*; Han, J. H., Ed.; Elsevier Academic Press: New York, NY, 2005; pp. 263–274.

(16) Brinker, C. J. Hydrolysis and condensation of silicates: effects on structure. *J. Non-Cryst. Solids* **1988,** *100,* 31–50.

(17) Brinker, C. J.; Scherer, J. W. *Sol-Gel Science: The Physics and Chemistry of Sol-Gel Processing*. Academic Press: New York, NY, 1990.

427 (18) Aelion, R.; Loebel, A.; Eirich, F. Hydrolysis of ethyl silicate. *J. Am. Chem. Soc.* **1950,** *72,*
428 5705–5712.
429 (19) Geppi, M.; Mollica, G.; Borsacchi, S.; Marini, M.; Toselli, M.; Pilati, F. Solid state NMR
430 characterization of PE-PEG/Silica hybrid materials prepared by microwave-assisted sol–
431 gel process. *J. Mater. Res.* **2007,** *22,* 3516–3525.
432 (20) Bandyopadhyay, A.; De Sarkar, M.; Bhowmick, A. Poly(vinyl alcohol)/silica hybrid
433 nanocomposites by sol-gel technique: synthesis and properties. *J. Mater. Sci.* **2005,** *40,*
434 5233–5241.
435 (21) Minelli, M.; De Angelis, M. G.; Doghieri, F.; Rocchetti, M.; Montenero, A. Barrier
436 properties of organic-inorganic hybrid coatings based on polyvinyl alcohol with
437 improved water resistance. *Polym. Eng. Sci.* **2010,** *50,* 144–153.
438 (22) ASTM. Standard practices for producing films of uniform thickness of paint, varnish, and
439 related products on test panels. Designation D823-07. American Society for Testing and
440 Materials. West Conshohocken PA 19428 – 2959 United States.
441 (23) Bell, L. N.; Labuza, T. P. *Practical Aspects of Moisture Sorption Isotherm Measurement*
442 *and Use*, 2nd ed.; AACC, Ed. Egan Press: Egan, MN, 2000.
443 (24) ASTM. Standard Test Method for oxygen gas transmission rate through plastic film and
444 sheeting using various sensors. Designation F 2622 – 08. American Society for Testing
445 and Materials. West Conshohocken PA 19428 – 2959 United States.
446 (25) Lee, D. S.; Yam, K. L.; Piergiovanni, L. *Food Packaging Science and Technology*. CRC
447 Press: Boca Raton, FL, 2008.
448 (26) Limpo, J.; Rubio, J.; Oteo, J. L. Estudio por FT-IR de la hidrolisis del tetraetilortosilicato.
449 *Bol. Soc. Esp. Ceram. V.* **1993,** *1,* 31–35.

(27) Shingel, K. I. Determination of structural peculiarities of dexran, pullulan and γ-irradiated pullulan by Fourier-transform IR spectroscopy. *Carbohyd. Res.* **2002,** *337,* 1445–1451.

(28) Uragami, T.; Okazaki, K.; Matsugi, H.; Miyata, T. Structure and permeation characteristics of an aqueous ethanol solution of organic-inorganic hybrid membranes composed of poly(vinyl alcohol) and tetraethoxysilane. *Macromolecules* **2002,** *35,* 9156–9163.

(29) Lee, S.-Y.; Lee, J.-D.; Yang, S.-M. Preparation of silica-based hybrid materials coated on polypropylene film. *J. Mater. Sci.* **1999,** *34,* 1233–1241.

(30) Tong, Q.; Xiao, Q.; Lim, L.-T. Preparation and properties of pullulan–alginate–carboxymethylcellulose blend films. *Food Res. Int.* **2008,** *41,* 1007–1014.

(31) Bhagat, S. D.; Hirashima, H.; Rao, A. V. Low density TEOS based silica aerogels using methanol solvent. *J. Mater. Sci.* **2007,** *42,* 3207–3214.

(32) Auras, R.; Harte, B.; Selke, S. Effect of water on the oxygen barrier properties of poly (ethylene terephthalate) and polylactide films. *J. Appl. Polym. Sci.* **2004,** *92,* 1790–1803.

(33) Hu, Y. S.; Mehta, S.; Schiraldi, D. A.; Hiltner, A.; Baer, E. Effect of water sorption on oxygen-barrier properties of aromatic polyamides. *J. Polym. Sci. Pol. Phys.* **2005,** *43,* 1365–1381.

(34) Minelli, M.; De Angelis, M. G.; Doghieri, F.; Marini, M.; Toselli, M.; Pilati, F. Oxygen permeability of novel organic–inorganic coatings: I. Effects of organic–inorganic ratio and molecular weight of the organic component. *Eur. Polym. J.* **2008,** *44,* 2581–2588.

(35) Farris S.; Introzzi L.; Biagioni, P.; Holz, T.; Schiraldi, A.; Piergiovanni L. Wetting of biopolymer coatings: contact angle kinetics and image analysis investigation. *Langmuir* **2011,** *27,* 7563–7574.

(36) Fabbri, P.; Singh, B.; Leterrier, Y.; Manson, J.-A. E.; Messori, M.; Pilati, F. Cohesive and adhesive properties of polycaprolactone/silica hybrid coatings on poly (methyl methacrylate) substrates. *Surf. Coat. Tech.* **2006,** *200,* 6706–6712.

(37) Kim, S.-W. Preparation and barrier property of poly (vinyl alcohol)/SiO_2 hybrid coating films. *Korean J. Chem. Eng.* **2008,** *25,* 1195–1200.

Tables

Table 1. Formulation, thickness and residual moisture of the coatings tested in this work

Exp. n°	Coded name	Pullulan (wt-%)	$Si(OH)_4$ (wt-%)	(O/I*) ratio	Coating thickness (μm)	Residual moisture (%)
1	H_0	10	0	/	1.27 ± 0.12^{a}	2.44 ± 0.05^{A}
2	H_3	7.5	2.5	3	1.37 ± 0.18^{ab}	2.61 ± 0.02^{AB}
3	H_2	6.66	3.33	2	1.31 ± 0.07^{ab}	2.78 ± 0.04^{BC}
4	H_1	5	5	1	1.26 ± 0.14^{ab}	2.71 ± 0.06^{CD}
5	$H_{0.75}$	4.3	5.7	0.75	1.19 ± 0.08^{ab}	2.57 ± 0.03^{D}
6	$H_{0.5}$	3.33	6.66	0.5	1.15 ± 0.09^{b}	2.66 ± 0.04^{E}

* "I" refers to the silanol form, $Si(OH)_4$, calculated by the initial TEOS content and assuming the completion of the hydrolysis reaction.
Different superscripts denote statistically significant differences within groups ($p < 0.05$).

Table 2. Parameters obtained from the fitting of the experimental sorption data with the GAB model (Equation 2) for the coating formulations H_0, H_3, and H_2 prepared at 25°C.

Coating type	R^2	M_0*	C	K
H_0 (pure pullulan)	0.991	0.78	0.03	1.06
H_3 (O/I=3)	0.997	0.53	0.03	1.07
H_2 (O/I=2)	0.995	0.19	0.08	1.04

* g/100g solids

Table 3. Oxygen Transmission Rate (OTR) of PET, and PET coated with pullulan and the hybrid coatings at five different relative humidity gradients and 23°C

Sample	Oxygen Transmission Rate (mL m^{-2} 24 h^{-1})				
	Relative humidity gradient (ΔRH, %)				
	0	20	40	60	80
PET	165.20^{a} (±1.96)	147.10^{g} (±1.65)	140.05^{l} (±0.873)	130.30^{s} (±1.05)	126.08^{x} (±2.14)
PET/H_0	4.92^{b} (±0.13)	5.95^{h} (±0.07)	9.98^{m} (±0.71)	54.60^{t} (±0.38)	106^{y} (±0.74)
PET/H_3	0.96^{c} (±0.03)	1.12^{c} (±0.01)	2.79^{n} (±0.19)	40.90^{q} (±0.20)	102^{z} (±0.30)
PET/H_2	5.23^{b} (±0.24)	6.48^{i} (±0.05)	11.40^{o} (±0.43)	54.20^{t} (±0.22)	105^{y} (±0.21)
PET/H_1	13.30^{do} (±0.39)	12.80^{d} (±0.30)	15.40^{p} (±0.45)	58.30^{u} (±0.12)	111^{A} (±0.22)
$PET/H_{0.75}$	31.90^{e} (±1.21)	33.90^{j} (±0.40)	41.30^{q} (±1.11)	85.70^{v} (±0.43)	110^{A} (±0.88)
$PET/H_{0.5}$	82.30^{f} (±1.97)	65.50^{k} (±0.19)	63.80^{r} (±1.08)	92.70^{w} (±0.46)	111^{A} (±1.22)

Different superscripts denote statistically significant differences ($p < 0.05$).

528 **Figure captions**

529

530

531 **Figure 1.** Representative chemical structure of pullulan as repeating units of maltotriose.

532

533 **Figure 2.** Schematic representation of the reactions expected in the sol-gel hybrid network
534 formation.

535

536 **Figure 3.** Optical microscope cross-section of PET film coated with a pullulan-silica hybrid
537 coating.

538

539 **Figure 4.** FTIR-ATR spectra of pullulan (a), reacted TEOS (b) and pullulan (□), reacted TEOS
540 (○), and hybrid coatings $H_{0.5}$ (——), $H_{0.75}$ (·····), H_1 (- - - -), H_2 (——), H_3 (——) within 1300
541 cm^{-1} – 850 cm^{-1} (c) and 3800 cm^{-1} – 3000 cm^{-1} (d) spectral ranges.

542

543 **Figure 5.** Sorption isotherm mean curves of pure pullulan coating (□ experimental data; **- - - -**
544 predicted data) and hybrid coatings H_3 (◇ experimental data; —— predicted data) and H_2 (△
545 experimental data; —— predicted data) at 25°C. The predicted data were obtained by fitting the
546 experimental points with the GAB model (Equation 2 in the text).

547

548 **Figure 6.** TEM images of reacted TEOS (a), pullulan (b), and the hybrid coating H_1 (c and d) at
549 two different magnifications. All images are from 0.5 wt-% hybrid dispersions 1 hour after
550 preparation.

551

552 **Figure 7.** OTR evolution for PET, pullulan, and the five hybrid coatings over the 0%–80%
553 relative humidity gradient range at 23°C.
554
555 **Figure 8.** Optical microscope images of coating surfaces at 10× magnification in normal (left)
556 and topographical (right) modes (with the exception of sample $H_{0.75}$, where a 20× magnification
557 of the normal mode image is reported).
558
559
560
561
562
563
564
565
566
567
568
569
570
571
572
573
574
575
576

Table of Contents

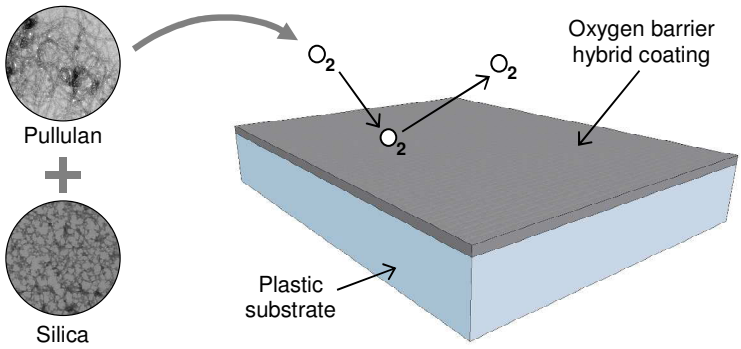

Table of Content categories:

1. Chemical Changes Induced by Processing/Storage
2. Environmental Chemistry
3. Chemical Aspects of Biotechnology/Molecular Biology

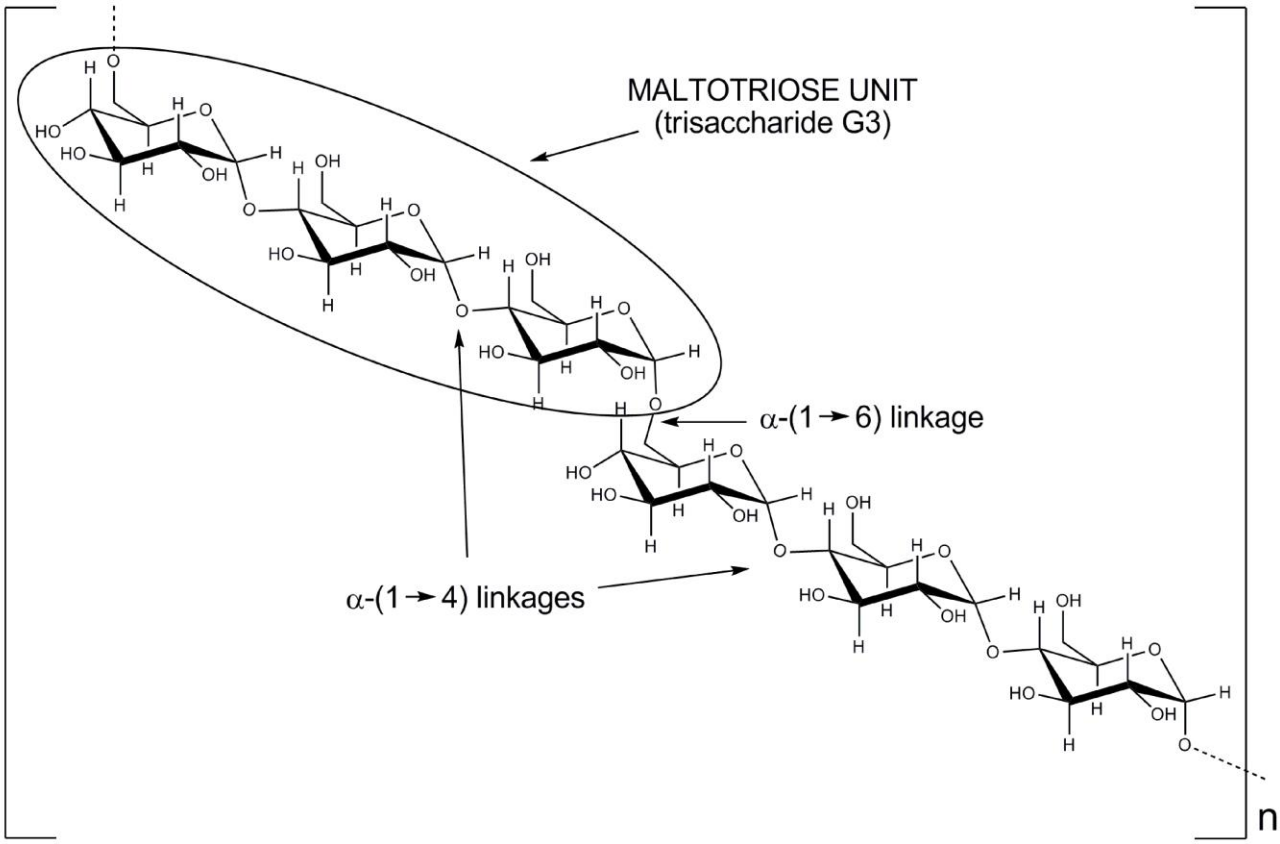

Figure 1. Representative chemical structure of pullulan as repeating units of maltotriose.

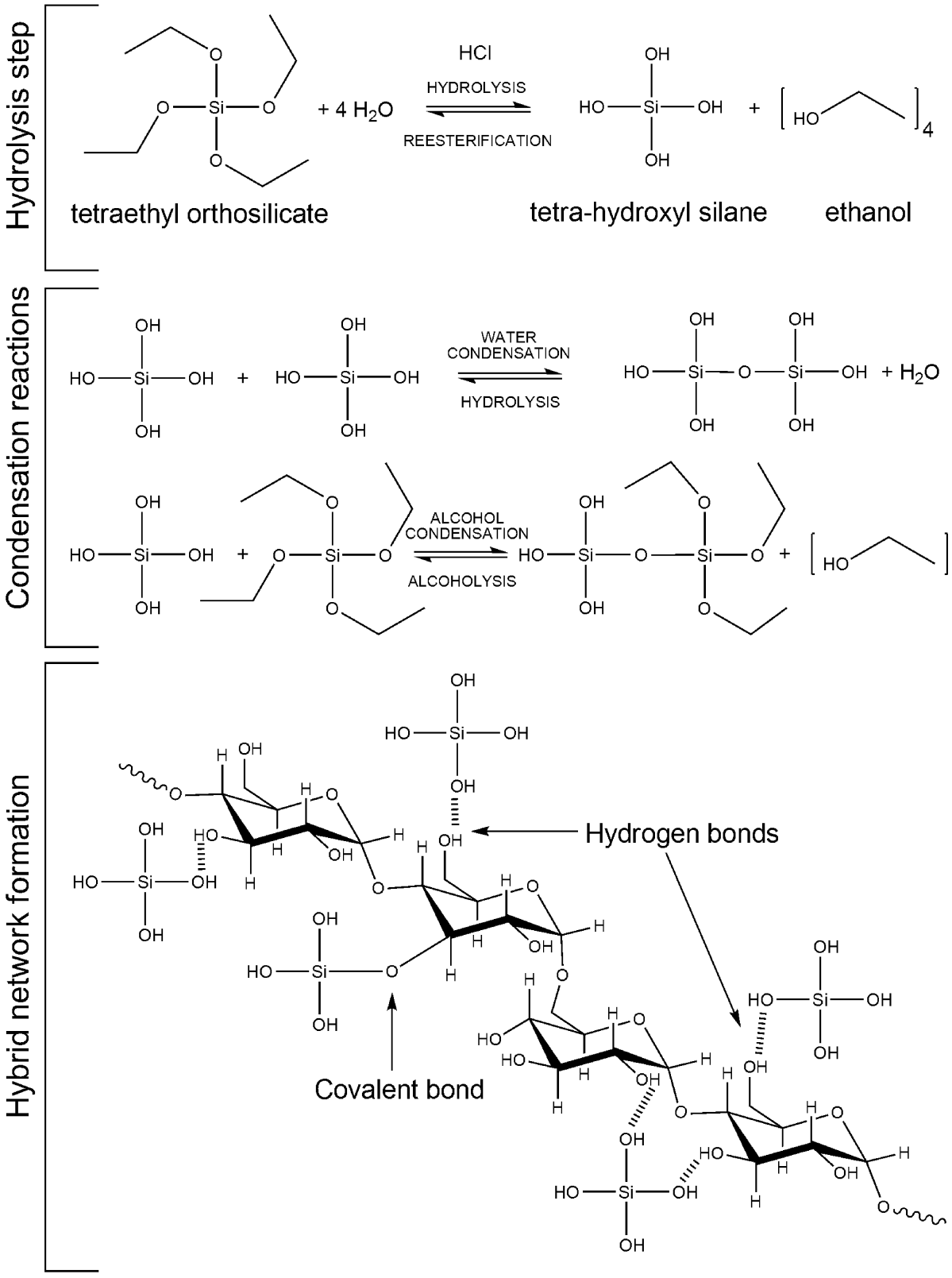

Figure 2. Schematic representation of the reactions expected in the sol-gel hybrid network formation.

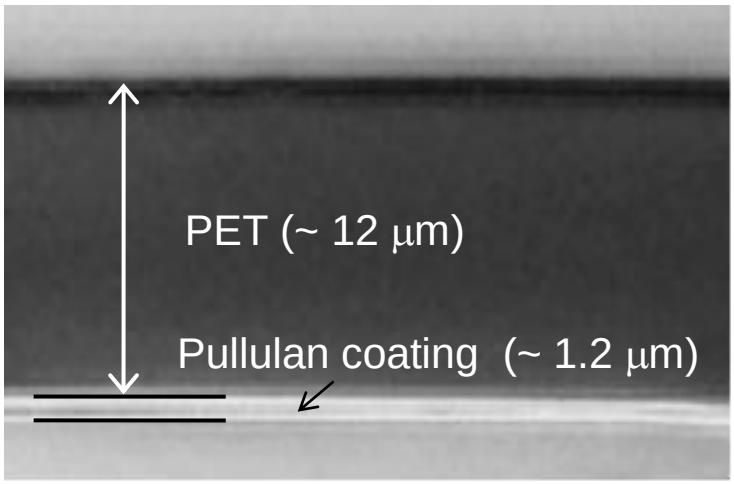

Figure 3. Optical microscope cross-section (50×) of PET film coated with a pullulan-silica hybrid coating.

a

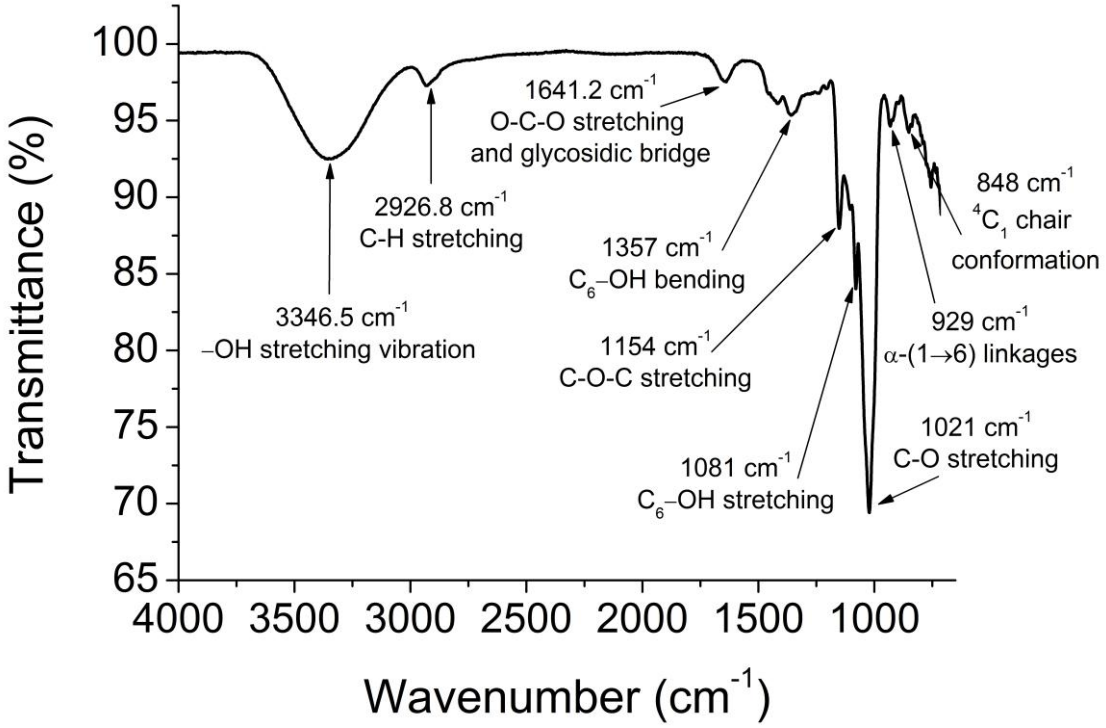
Transmittance (%)
Wavenumber (cm-1)
1641.2 cm-1
O-C-O stretching
and glycosidic bridge
2926.8 cm-1
C-H stretching
3346.5 cm-1
–OH stretching vibration
1357 cm-1
C6–OH bending
1154 cm-1
C-O-C stretching
1081 cm-1
C6–OH stretching
848 cm-1
4C1 chair
conformation
929 cm-1
α-(1→6) linkages
1021 cm-1
C-O stretching

b

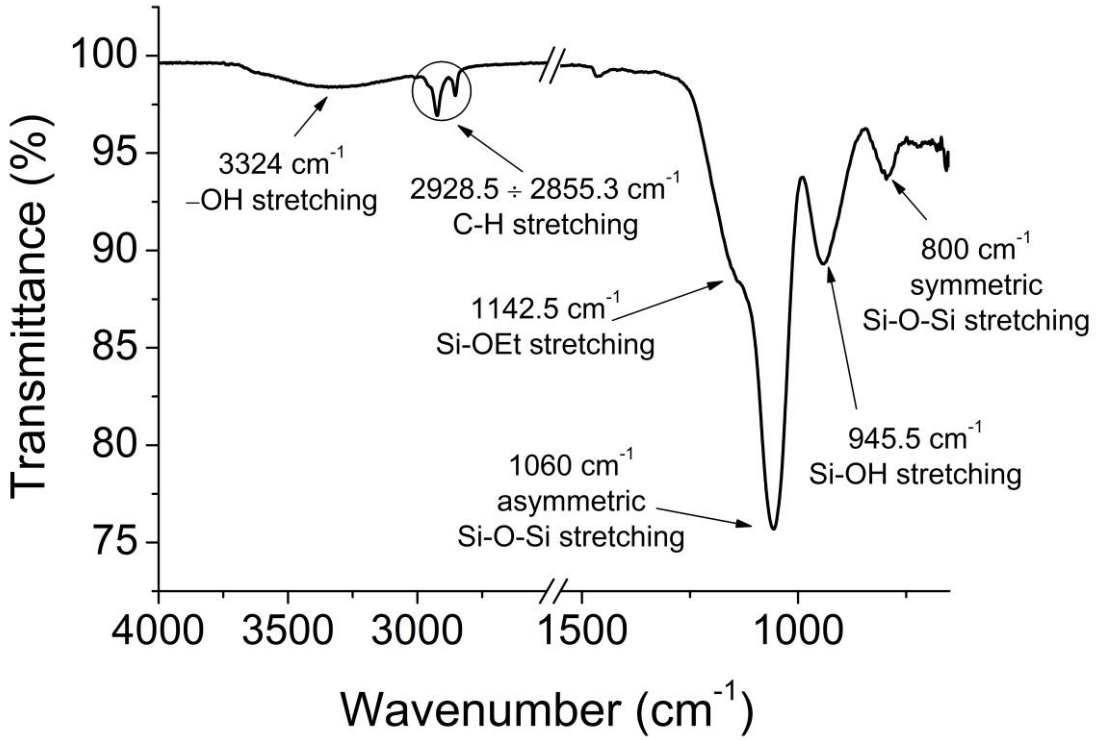
Transmittance (%)
Wavenumber (cm-1)
3324 cm-1
–OH stretching
2928.5 ÷ 2855.3 cm-1
C-H stretching
1142.5 cm-1
Si-OEt stretching
1060 cm-1
asymmetric
Si-O-Si stretching
945.5 cm-1
Si-OH stretching
800 cm-1
symmetric
Si-O-Si stretching

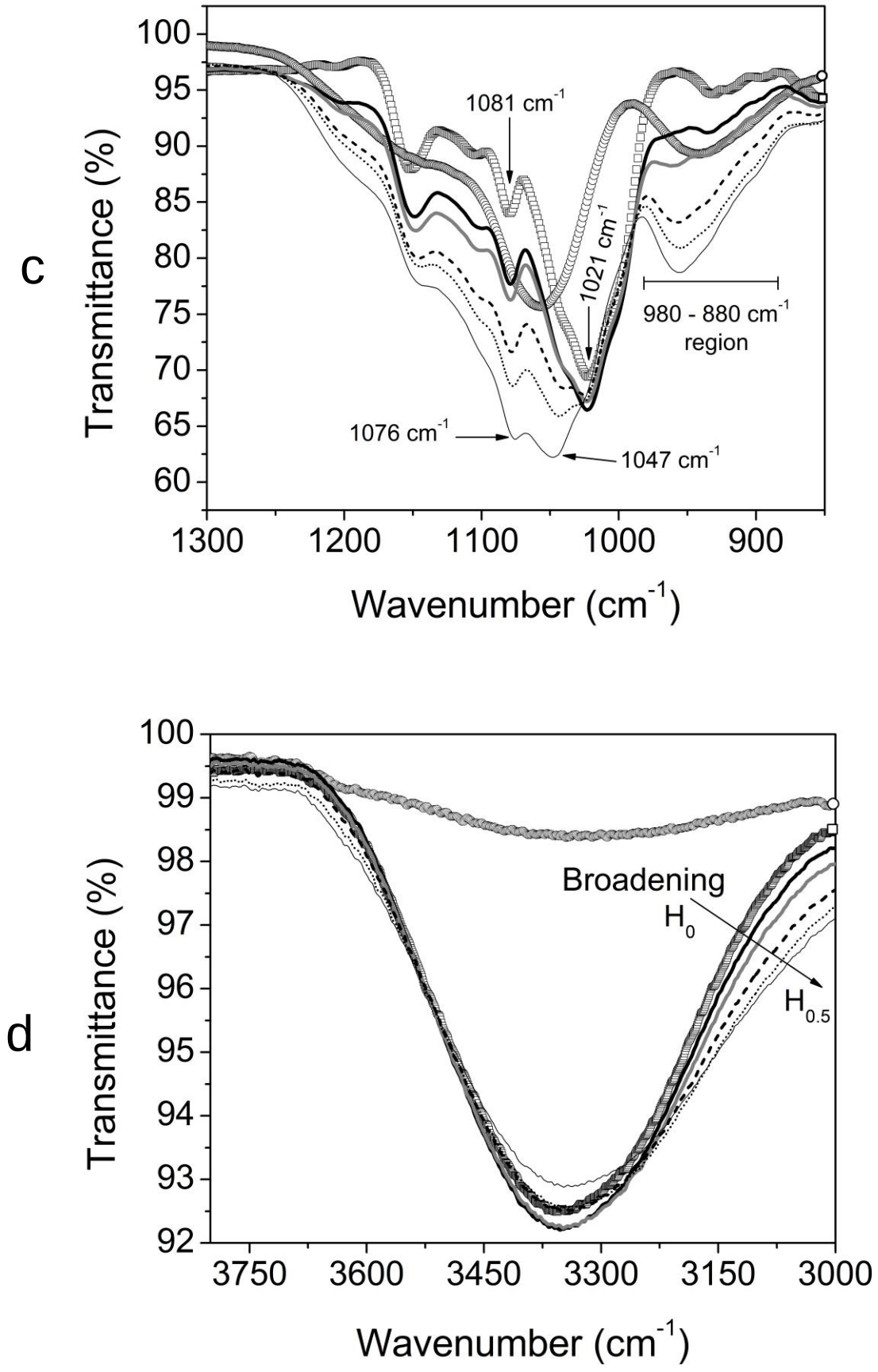

Figure 4. FTIR-ATR spectra of pullulan (a), reacted TEOS (b) and pullulan (□), reacted TEOS (○), and hybrid coatings $H_{0.5}$ (——), $H_{0.75}$ (·····), H_1 (- - - -), H_2 (———), H_3 (——) within 1300 cm^{-1} – 850 cm^{-1} (c) and 3800 cm^{-1} – 3000 cm^{-1} (d) spectral ranges.

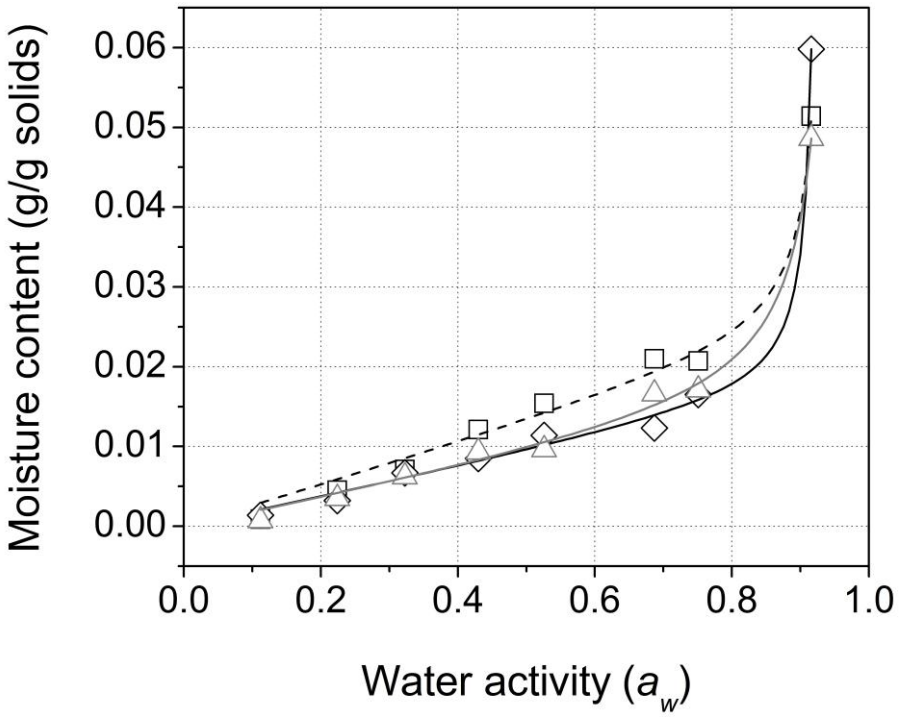

Figure 5. Sorption isotherm mean curves of pure pullulan coating (□ experimental data; - - - - predicted data) and hybrid coatings H_3 (◇ experimental data; —— predicted data) and H_2 (△ experimental data; —— predicted data) at 25°C. The predicted data were obtained by fitting the experimental points with the GAB model (Equation 2 in the text).

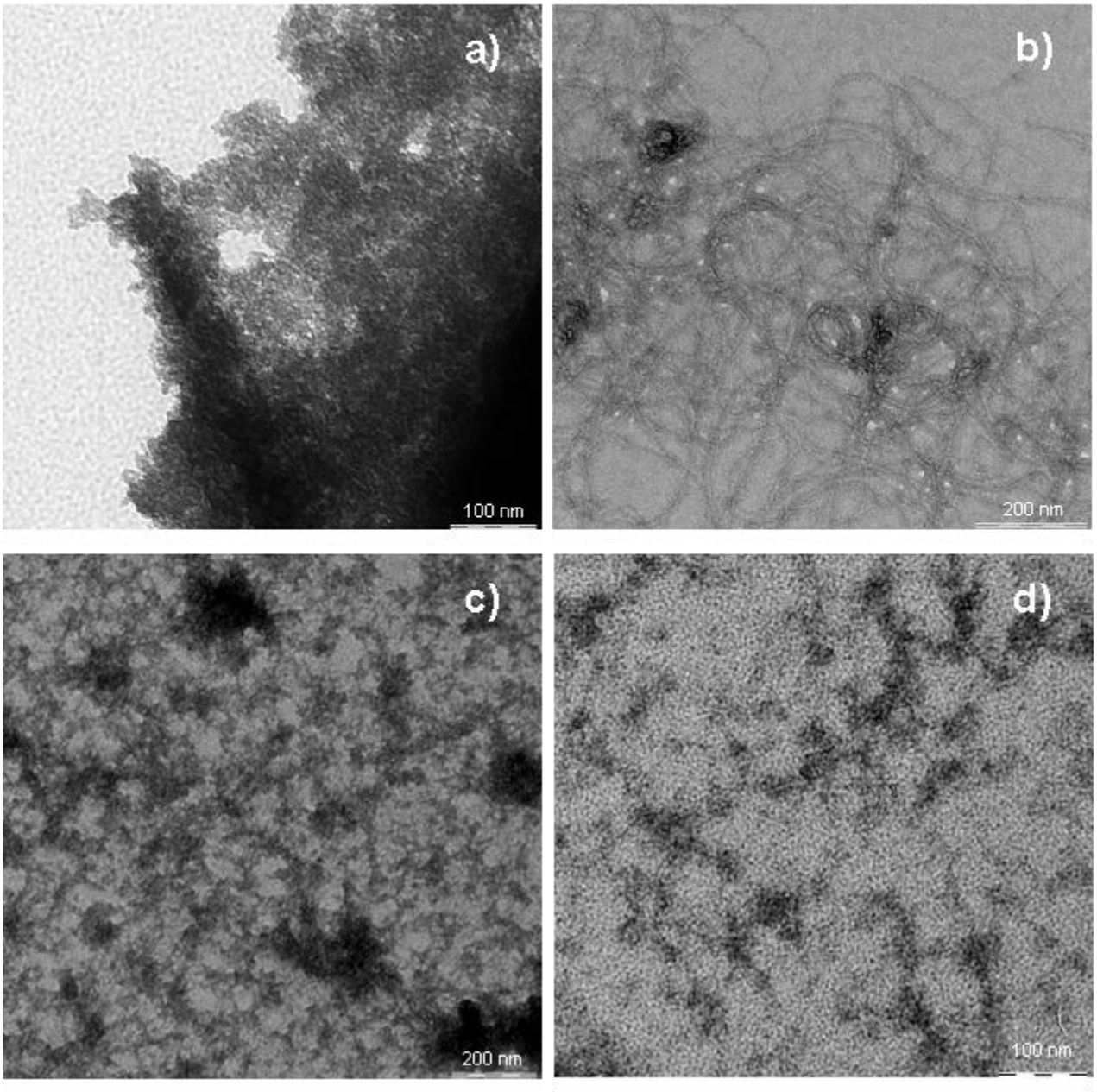

Figure 6. TEM images of reacted TEOS (a), pullulan (b), and the hybrid coating H_1 (c and d) at two different magnifications. All images are from 0.5 wt-% hybrid dispersions 1 hour after preparation.

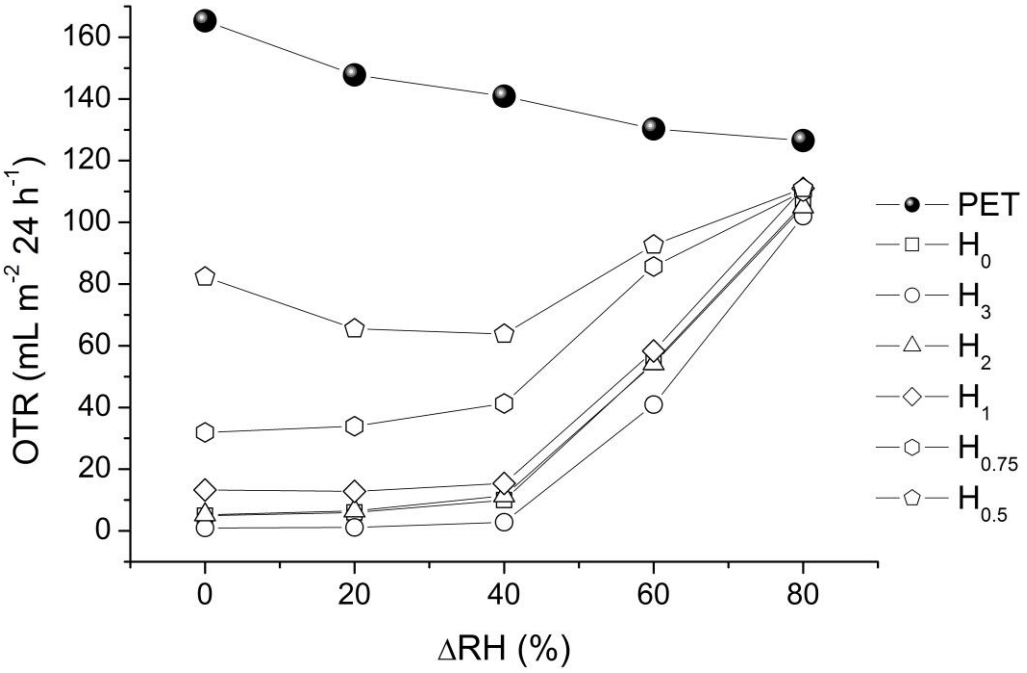

Figure 7. OTR evolution for PET, pullulan, and the five hybrid coatings over the 0%–80% relative humidity gradient range at 23°C.

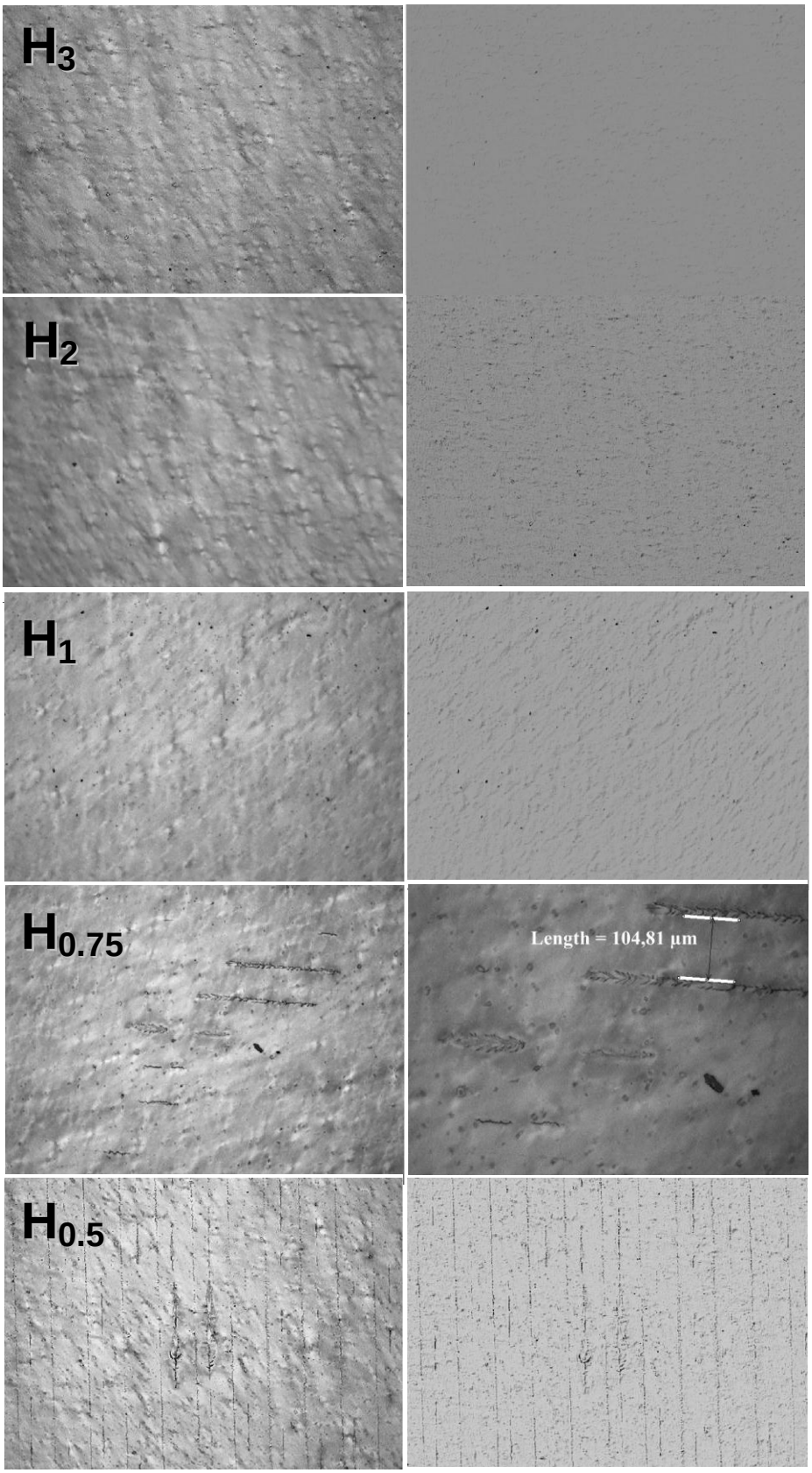

Figure 8. Optical microscope images of coating surfaces at 10× magnification in normal (left) and topographical (right) modes (with the exception of sample $H_{0.75}$, where a 20× magnification of the normal mode image is reported).